Linear time-continuous state-space realization of flame transfer functions by means of a propagation equation

Philipp Brokof[1], Guillaume J. J. Fournier[2], Wolfgang Polifke[3]
Technical University of Munich,
TUM School of Engineering and Design,
Department of Engineering Physics and Computation
Boltzmannstr. 15, 85747 Garching, Germany

ABSTRACT

Low-order network models, commonly used to assess the thermo-acoustic stability of combustors, can be cast in a linear, time-continuous state-space representation. A standard linear eigenvalue problem for the system modes results, which can be solved in a robust and efficient manner. To represent the linear dynamics of any time-invariant flame in the state-space framework, this study presents an approximation of the distributed-time-delayed flame response to acoustic velocity perturbations based on a spatially discretized propagation equation (PE). We derive the rational flame transfer function of a first-order-upwind-PE state-space model and discuss its relation to the Tustin approximation of transfer functions. For an exemplary discrete finite impulse response of a flame, a third-order-upwind-PE state-space model is shown to match the discrete flame frequency response with an accuracy comparable to that of a rational approximation found by non-linear optimization. The numerical dissipation introduced by discretization of the PE ensures negligible gain above the Nyquist frequency of the underlying discrete flame impulse response. Finally, we apply the PE state-space flame model to a generic Rijke tube and show that the predicted thermo-acoustic modes agree well with results obtained from a classical non-linearly optimized rational approximation of the frequency response function of the flame.

1. INTRODUCTION

Thermo-acoustic instability problems involve length scales ranging from acoustic wave lengths in the order of the dimensions of the combustion device to flame thicknesses of a few millimeters [1]. To predict the stability of a combustor with reasonable computational effort, a common strategy is to divide the problem into sub-models with tailored complexity. Flame transfer functions (FTF) stemming from high-fidelity simulations can be incorporated into low-order acoustic networks [2]. Similarly, acoustic network models can be applied as boundary conditions in high-fidelity simulations to reduce the size of the computational domain [3].

[1]philipp.brokof@tum.de

[2]guillaume.fournier@tum.de

[3]polifke@tum.de

Thermo-acoustic low-order networks usually lead to a non-linear eigenvalue problem for the system dynamics, i.e. system modes and their corresponding frequencies and growth rates. This non-linear eigenvalue problem is mainly a result of the phase shift experienced by acoustic waves traveling through the geometry and the distributed-time-delayed reactions [4] of flames to acoustic velocity perturbations, both leading to terms where the (complex-valued) frequency occurs in the exponent of the exponential function. Furthermore, non-linearities can be introduced by non-trivial boundary conditions, represented by complex-valued reflection coefficients, and acoustic inertia in models of acoustically compact elements, e.g. for long holes in [5]. Solving this non-linear eigenvalue problem by iterative root-finding [6] is computationally expensive. More crucial, the choice of the initial conditions for the search algorithm [7] determines which modes are found, and there is no guarantee that one finds *all* roots of the system. Contour integral methods, which ensure that all eigenmodes within a contour in the complex-plane are found, offer a remedy [7]. However, these methods remain computationally expensive [8].

Schuermans et al. [9] introduced the state-space approach to acoustic modeling, based on a modal expansion technique and sub-model interconnection by the Redheffer Star Product. Emmert at al. [10], on the other hand, connect sub-models with a feed-through equation. State-space formulations for network elements are deduced from rational polynomials that represent the respective transfer functions or from a spatial discretization of a propagation equation. If the state-space models of all individual elements are linear, the resulting state-space model of the overall acoustic network is also linear and a linear eigenvalue problem results, which can be solved in a robust and efficient manner. This is an important advantage of state-space models over the standard formulation of network models [8, 11].

The crucial point is the formulation of linear state-space models for network elements with time-delays/phase shifts. For example, for a duct element, the characteristic amplitudes of acoustic waves entering and leaving the duct can be set as the inputs and outputs of the state-space model, respectively. Since the acoustic waves simply propagate through the duct, leading to a phase shift, a linearized description of the system dynamics can be obtained by discretizing the propagation equation (PE) in space [10].

The n-τ flame model shows great similarity to the aforementioned duct element if the time-delay is interpreted as the time that the input to the model (acoustic velocity perturbation) needs to propagate through a pseudo space until it affects the output of the model (heat release perturbation). The length of the pseudo space and the propagation speed of the perturbation are matched to the desired time-delay of the flame. In literature, states stemming from the discretization of the pseudo space are referred to as "lagged states" [12] or "history states" [13]. The PE was used to realize the n-τ model into state-space by Meindl et al. [11], and Mangesius and Polifke [13]. However, Schmid et al. [14] point out that the n-τ model should only be used if the absolute time lag of the flame is known and Subramanian et al. [12] advocate for distributed time-delay response functions to capture the rich complexity of flame dynamics.

More sophisticated descriptions of flame dynamics can be obtained by (1) harmonic forcing of the flame to identify the frequency response function (FRF) or (2) broad-band excitation and a correlation analysis to identify the impulse response of the flame. However, an analytic time-continuous description of frequency response function (FRF) or impulse response cannot be obtained from these system identification (SI) techniques. The FRF will only be available at discrete frequencies and the impulse response will consist of a truncated series of discrete impulses, also known as finite impulse response (FIR). However, we require a time-continuous state-space (CSS) model for stability analysis. The advantage of such a time-continuous model is the possibility of coupling with a variable time step computational fluid dynamics (CFD) simulation, allowing an efficient implementation of time domain impedance boundary conditions [3, 15]. Common strategies to obtain CSS models from discrete FRF data are (1) fitting a rational function [12, 16–18], or (2) first-order bilinear/Tustin and higher-order Padé approximation [9, 19] of exponential terms. For either method, the obtained rational function is subsequently transformed into a CSS model, e.g. in Jordan canonical form [20].

The contribution of the present study is to formulate a PE based CSS model for arbitrary FIRs. Furthermore, an analytic analysis of the model is given and its performance is compared to the rational-fitting strategy for an example FIR of a laminar premixed flame [21] obtained by SI [2]. In this study, the FIR is taken as input and details on its computation are out of the scope of the presentation.

This paper is organized as follows: Section 2 reviews common low-order representations of flames, i.e. FIR and FTF. Subsequently, Section 3 introduces the PE based CSS realization of flame transfer functions. In Section 4, the performance of the presented PE CSS model is compared with a CSS based on rational-fitting. Both CSS models are compared regarding the recovery of the discrete frequency response of the flame, and the influence of the CSS realization strategy on the eigenvalues of a generic Rijke tube is assessed. Finally, Section 5 concludes this study with a summary of the findings.

2. LOW-ORDER FLAME MODELS IN THERMO-ACOUSTICS

This section reviews the concepts of flame impulse response and flame transfer function. We point out the interrelation between frequency and time domain in both, the time-discrete and time-continuous case. A graphical overview of the different domains can be found in [4], Figure 2.

The discrete response series r_l of a causal linear system to any discrete signal series s_l can be obtained by convolution of the signal with the system's FIR $\mathbf{h} = (h_0, h_1, ..., h_N)$ of length N. For a velocity sensitive flame, the input signal consists of the normalized velocity perturbation $u'/\bar{u}$ at a reference point and the response of interest is the normalized fluctuating heat release $\dot{Q}'/\overline{\dot{Q}}$ of the flame. For harmonic input signals $s_l = \hat{u}/\bar{u}e^{s\Delta tl}$, the discrete FTF $\mathcal{F}_d(s)$ that corresponds to the FIR $\mathbf{h}$ becomes

$$r_l = \sum_{k=0}^{N} h_k \frac{\hat{u}}{\bar{u}} e^{s\Delta t(l-k)} = \frac{\hat{u}}{\bar{u}} e^{s\Delta tl} \sum_{k=0}^{N} h_k e^{-s\Delta tk} \Rightarrow \mathcal{F}_d(s) = \frac{\hat{\dot{Q}}/\overline{\dot{Q}}}{\hat{u}/\bar{u}} = \sum_{k=0}^{N} h_k e^{-s\Delta tk}, \tag{1}$$

where $s = \sigma + i\omega$ is the Laplace variable and $\hat{(\cdot)}$ denotes the complex amplitude. From Eq. (1), it is evident that the FTF can be interpreted as the sum of the distributed-time-delayed responses of the flame to impulse forcing and is non-linear in s.

The discrete equivalent to the Laplace transform is the z-transform. By substituting $z = e^{s\Delta t}$ in Eq. (1), we find that the z-transform of the FIR equals the FTF. A rational approximation of $\mathcal{F}(s)$ can be found by setting

$$z = \frac{e^{s\frac{\Delta t}{2}}}{e^{-s\frac{\Delta t}{2}}} \approx \frac{1 + \frac{\Delta t}{2}s}{1 - \frac{\Delta t}{2}s}, \tag{2}$$

which is known as bilinear transform or Tustin transform [22]. The Tustin transform keeps the mapping properties of the exponential function between Laplace and z-space and, therefore, conserves stability properties of the time-discrete model when used to find a time-continuous description and vice versa. Equation (2) shows that the Tustin transform, which is the first-order Padé approximation [23], is based on the first-order Taylor series expansion $e^x \approx 1 + x$. Hence, accuracy can only be expected for sufficiently small frequencies or small time increments Δt. Rational approximations of the time-delay term for higher frequencies were achieved in [9, 19] using Padé approximations of higher orders.

3. CONTINUOUS STATE-SPACE REALIZATION BY PROPAGATION EQUATION

This sections presents a CSS realization based on a PE. We start with a minimal example and realize a FIR consisting of three impulses in a first-order-upwind-PE CSS model. Subsequently, the equivalent continuous flame transfer function is generalized for arbitrary FIRs. From this generalization, the stability and mapping properties from z-space to Laplace space of the first-order-upwind-PE CSS model are assessed.

3.1. Minimal Example

Let us assume a FIR consisting of three impulses, $\mathbf{h} = (h_0, h_1, h_2)$, as shown in Figure 1. The FIR is sampled with a constant time increment Δt. Let the pseudo space in Θ be discretized with $\Delta\Theta = \Delta t/2$. The flame responds instantaneously with h_0 to the velocity perturbation signal $u'/\bar{u}$, but the signal has to travel the distance $2\Delta\Theta = \Delta t$ with unity propagation speed through the pseudo space until the time-delay corresponding to h_1 has passed. Similarly, the signal has to travel twice the distance until the time-delay of h_2 has passed. Introducing history states $\mathbf{x} = (x_1, ..., x_4)^T$, which store the signal at different positions in pseudo space, the evolution of the state variables $\mathbf{x}$ is completely described by a PE. Rearranging the PE for the time derivative of x and discretizing the spatial derivative with a first-order upwind finite difference stencil yields

$$\frac{\partial x}{\partial t} = -\frac{\partial x}{\partial \theta} \approx -\left[\frac{x_i - x_{i-1}}{\Delta\theta}\right]. \tag{3}$$

Application of Eq. (3) to all states $\mathbf{x}$ gives

$$\begin{pmatrix} \dot{x}_1 \\ \dot{x}_2 \\ \dot{x}_3 \\ \dot{x}_4 \end{pmatrix} = \underbrace{\begin{pmatrix} -\frac{1}{\Delta\Theta} & 0 & 0 & 0 \\ \frac{1}{\Delta\Theta} & \frac{-1}{\Delta\Theta} & 0 & 0 \\ 0 & \frac{1}{\Delta\Theta} & \frac{-1}{\Delta\Theta} & 0 \\ 0 & 0 & \frac{1}{\Delta\Theta} & \frac{-1}{\Delta\Theta} \end{pmatrix}}_{\mathbf{A}} \begin{pmatrix} x_1 \\ x_2 \\ x_3 \\ x_4 \end{pmatrix} + \underbrace{\begin{pmatrix} \frac{1}{\Delta\Theta} \\ 0 \\ 0 \\ 0 \end{pmatrix}}_{\mathbf{B}} \frac{u'}{\bar{u}}, \tag{4}$$

where $\mathbf{A}$ is the system matrix and $\mathbf{B}$ is the input matrix. We can formulate the output equation for fluctuating heat release as

$$\frac{\hat{\dot{Q}}}{\bar{\dot{Q}}} = \underbrace{\begin{pmatrix} 0 & h_1 & 0 & h_2 \end{pmatrix}}_{\mathbf{C}} \begin{pmatrix} x_1 \\ x_2 \\ x_3 \\ x_4 \end{pmatrix} + \underbrace{h_0}_{\mathbf{D}} \frac{\hat{u}}{\bar{u}}, \tag{5}$$

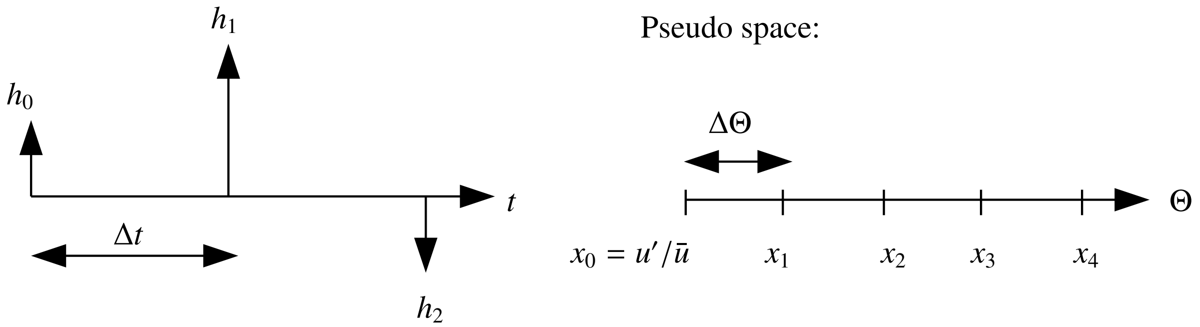

Figure 1: Minimal example: FIR consisting of three discrete impulses. Pseudo space is resolved with $\Delta\theta = \Delta t/2$.

where $\mathbf{C}$ and $\mathbf{D}$ are the output and feed-through matrix, respectively. Equations (4) and (5) form a continuous state-space model $(\mathbf{A}, \mathbf{B}, \mathbf{C}, \mathbf{D})$ with scalar input $\hat{u}/\bar{u}$ and scalar output $\hat{\dot{Q}}/\overline{\dot{Q}}$.

3.2. Analysis of the Resulting Flame Transfer Function

The system matrix $\mathbf{A}$ resulting from the first-order upwind discretization is triangular, allowing straightforward determination of its eigenvalues that characterize the dynamics of the CSS model. Note that the system matrix depends only on the discretization scheme and pseudo space resolution, and not on the impulse response $\mathbf{h}$. Furthermore, the coefficients of the system matrix are constant and frequency independent.

Equations (4) and (5) can be Laplace transformed and rearranged to find the corresponding continuous flame transfer function

$$\mathcal{F}(s)_{\Delta\Theta=\frac{\Delta t}{m}} = \frac{\hat{\dot{Q}}/\overline{\dot{Q}}}{\hat{u}/\bar{u}} = \mathbf{C}(s\mathbf{I}-\mathbf{A})^{-1}\mathbf{B}+\mathbf{D} = \sum_{k=0}^{N} \frac{h_k}{\left[s\frac{\Delta t}{m}+1\right]^{km}}, \tag{6}$$

where the parameter m controls the resolution of the pseudo space and N is the length of the FIR. Equation (6) shows that the corresponding FTF is a rational function with only stable poles of multiplicity mk at $s = -m/\Delta t$. Furthermore, for higher resolution of the pseudo space, the poles move to a strongly damped region that is not of concern for the stability analysis of thermo-acoustic systems.

Comparison with Eq. (1) shows that Eq. (6) is obtained from the exact FTF by substituting

$$z = e^{s\Delta t} = e^{s\frac{\Delta t}{m}m} = (e^{s\frac{\Delta t}{m}})^m \approx \left[s\frac{\Delta t}{m}+1\right]^m \Rightarrow z(i\omega) = \left[1+\left(\frac{\omega\Delta t}{m}\right)^2\right]^{m/2} e^{i\mathrm{atan}(\frac{\omega\Delta t}{m})m}. \tag{7}$$

Thus, the first-order-upwind-PE CSS model is, as the Tustin transform, based on a first-order Taylor series expansion of the exponential function. However, compared to the Tustin transform, the exponent is scaled by $1/m$ resulting in better performance at higher frequencies. For a fine resolution of the pseudo space, Eq. (7) recovers the mapping properties of the z-transform. This is evident from the complex pointer representation of the mapping. For high values of m, $|z(i\omega)| \to 1$, so that the imaginary axis is mapped on the unit circle.

4. COMPARISON OF PE AND DATA-FITTING BASED CSS MODELS

In this section, the performance of the PE CSS model is compared with a rational fit based CSS, where the sixth-order rational fit was obtained with the MATLAB [24] *tfest* function, requiring a quality of 99 % and constraining the poles to be stable. For further information about the rational fit CSS model, the reader is referred to [12, 16–18]. We assess (1) the mean square error (MSE) of the continuous frequency response function to the original discrete model and (2) the influence of the CSS realization strategy on the eigenvalues of a generic Rijke tube. The FIR for flame modeling consists of $N = 44$ discrete impulses and was obtained by SI from the simulation of a Kornilov flame [21]. It is indicated in Figure 3 with blue dots.

4.1. Recovery of Discrete Flame Transfer Function

The difference between the FRF F_c of the CSS models and the original discrete FRF F_d is measured by the mean square error (MSE) in the complex plane over all N_d frequencies of the discrete model, i.e.

$$\mathrm{MSE} = \frac{1}{N_d}\sum_{k=1}^{N_d}\left|F_{d,k}-F_{c,k}\right|^2. \tag{8}$$

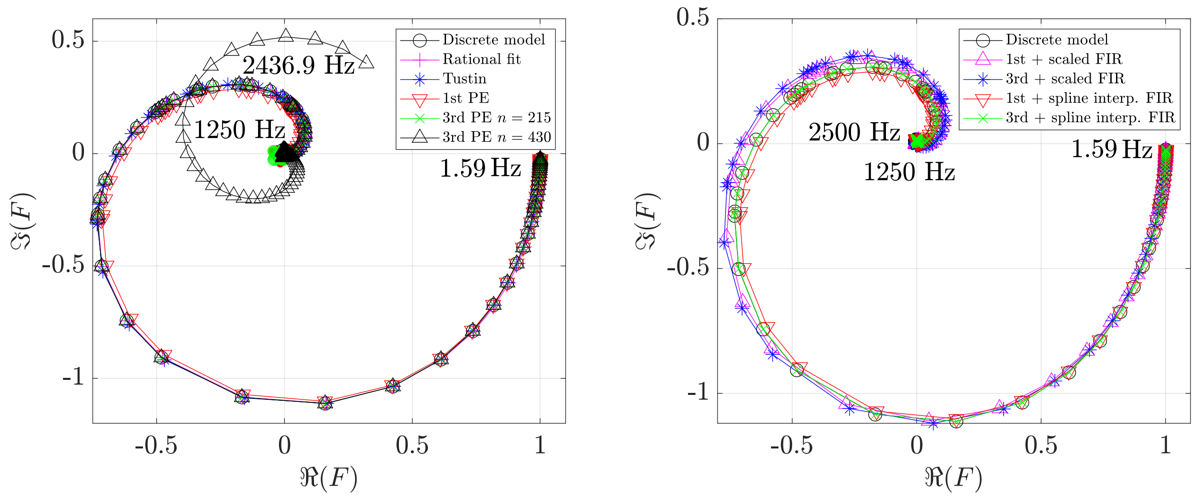

Figure 2: Left: Comparison between loci of discrete frequency response and continuous frequency responses from different CSS realizations. Right: Loci of frequency responses of PE CSS models based on resampled FIR.

The loci of the compared FRFs are shown in the left part of Figure 2. Note that the discrete model is only plotted up to its Nyquist frequency $f = 1/(2\Delta t) = 1250$Hz. The performance of the Tustin CSS model is good at low frequencies but severe deviations to the discrete model can be observed in phase for higher frequencies (the locations of markers on the parametric curve do not coincide with those of the discrete model). However, at high frequencies the gain of the FRF is low so that even big discrepancies in phase become unimportant. This is reflected by the low error of MSE = $7.16e^{-4}$. Per construction, the number of states of the Tustin model equals the number of time-delayed impulses in the FIR. The rational fit CSS model, with only six states, shows a small error of MSE = $1.34e^{-5}$, justifying its frequent use in literature. To achieve an error MSE = $1.09e^{-4}$, hence of the same order as for the Tustin CSS model, with the first-order-upwind-PE CSS model introduced in Section 3, the number of states increases drastically to 860. Remedy can be found by increasing the order of the upwind stencil for the PE discretization from first-order to third-order. The third-order-upwind-PE CSS model with 215 states shows an error of MSE = $1.51e^{-7}$, and a more accurate fit of the phase than the first-order-upwind-PE model. However, the system matrix of the third-order-upwind-PE CSS model is not triangular anymore, leading to a complex pole pattern of the corresponding rational FTF (in contrast to Eq. (6)).

Inspection of Figure 2 (left) reveals that the PE CSS models show spurious gain above the Nyquist frequency of the underlying discrete model. This is more significant for the third-order scheme and becomes even more significant if the number of states of the third-order model is increased from $n = 215$ to $n = 430$. In a frequency domain analysis, this spurious gain can be ignored since it occurs above the frequency range of interest, i.e. above the Nyquist frequency. However, in a time domain analysis that couples the CSS model to unsteady CFD [3, 15], this nonphysical behavior at higher frequencies would be present. The discrete model is only valid up to its Nyquist frequency of $f \approx 1250$ Hz. For higher frequencies, the z-transformed FRF is symmetric in magnitude and anti-symmetric in phase around this Nyquist frequency [4]. Hence, a continuous extrapolation based on the discrete model is expected to show symmetric high frequency peaks in gain. The spurious gain is damped only as a beneficial side effect of the numerical dissipation of the discretization scheme used in the PE CSS model.

To overcome this problem, we resample the FIR at every history state to increase the Nyquist frequency and push the (symmetric) spurious peak to higher frequencies where the numerical damping is stronger. In Figure 3 (left), additional sampling points are inserted and the FIR is step-wise rescaled to ensure a constant total impulse of the response. In Figure 3 (right), the original FIR was converted

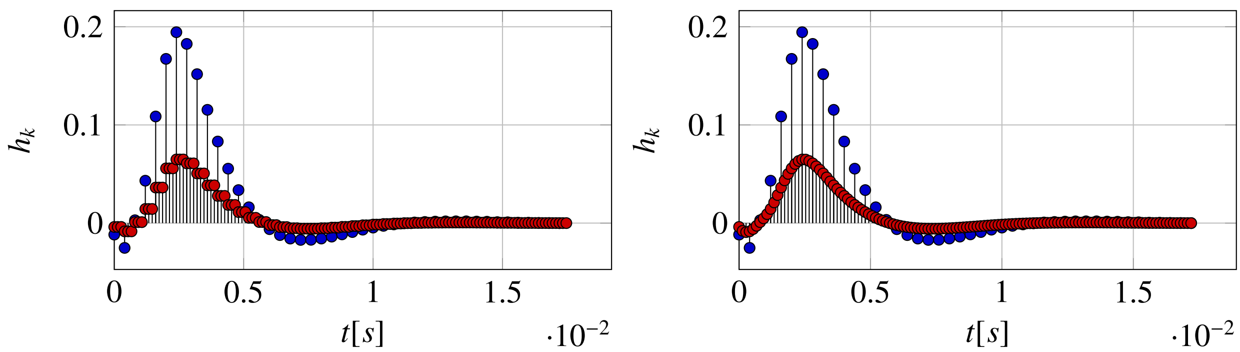

Figure 3: Comparison of different refinement strategies of the FIR: Scaling of the FIR (left) and scaling with spline interpolation (right).

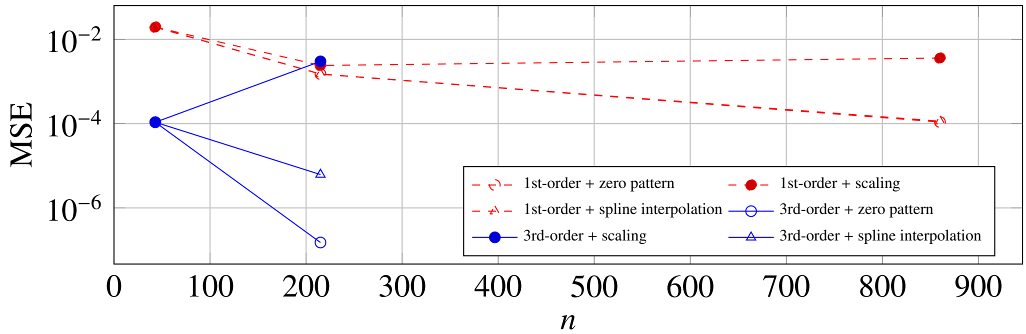

Figure 4: MSE to discrete model for increasing number of state variables n for resampled and original PE CSS models.

to a time series with a hold function, spline interpolated, and converted back to an impulse series under consideration of the finer sampling time.

Figure 2 (right) shows that for both resampling strategies the spurious gain observed before between 1250 Hz and 2500 Hz is suppressed. Inspection at frequencies up to twice of the new Nyquist limit showed no further peak in gain. The mere scaling strategy recovers the phase of the discrete model only at low frequencies. Figure 3 (left) shows that the scaling operation delays the overall impulse response. Since the phase of the FRF is closely related to the time-delay of the FIR, this effect becomes visible in the unmatched phase. In contrast, the phase accuracy of the spline-interpolated third-order-upwind-PE CSS is excellent. Figure 4 compares the MSEs of the resampled PE CSS models with the original PE CSS model, where the output matrix $\mathbf{C}$ was zero patterned, see Eq. (5). For the same number of states n, the error for the spline interpolation strategy is one order of magnitude higher than for the original zero patterning strategy in case of the third-order-upwind-PE CSS model. The phase accuracy of the merely scaled CSS model is poor and it is not guaranteed that the model's accuracy improves with increased number of states.

4.2. Influence of the CSS Realization on the Eigenvalues of a Rijke Tube

So far, the PE CSS model was only assessed for zero growth rate by limiting the analysis to the FRF. However, as pointed out by Schmid et al. [14], for linear stability analysis we have to solve the eigenvalue problem in the complex plane. The PE CSS model is a linear approximation of the time-delayed dynamics of the flame. Thus, the linear eigenvalue problem can only be expected to give similar eigenvalues as the original non-linear problem if this approximation is sufficiently good in the complex plane [8, 14].

Figure 5 shows magnitude and phase of the flame transfer functions $\mathcal{F}$ of the original distributed time-delay model according to Eq. (1), the third-order-upwind-PE CSS model with spline-interpolated

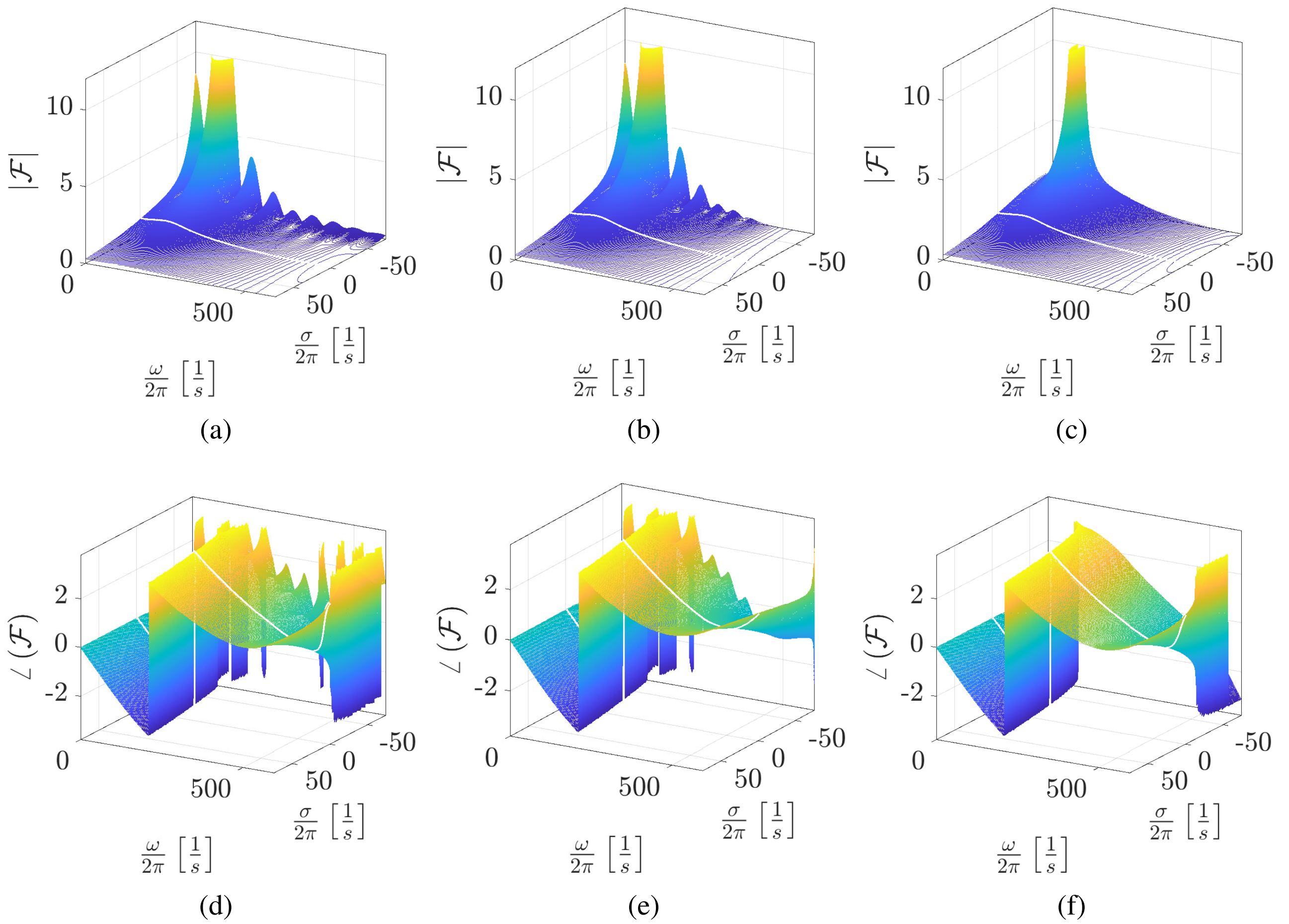

Figure 5: Magnitude and phase of the flame transfer functions $\mathcal{F}$ of the original distributed time-delay model according to Eq. (1) (a, d), 3rd-order-upwind-PE CSS model with spline-interpolated FIR (b, e) and 6th-order rational fit CSS model (c, f). The frequency response function (FRF) at zero growth rate is indicated by a white line.

FIR and the sixth-order rational fit CSS model. Although the fit of the FRF by the rational fit model was excellent, the FTF in the complex plane varies qualitatively from the FTF of the distributed time-delay model for normalized growth rates $\sigma/(2\pi) < -50$ 1/s. On the other hand, the FTF of the third-order-upwind-PE CSS is qualitatively more similar to the FTF of the distributed time-delay model.

To assess the linear approximation of the FTF obtained with the third-order-upwind-PE CSS model, we compute the eigenvalues of a one-dimensional Rijke tube with quiescent flow as shown in Figure 6 and compare them with the eigenvalues computed based on the rational fit CSS. Only planar one-dimensional acoustic waves are non-evanescent and the waves travelling between network elements are indicated with curved arrows in Figure 6. Both ends of the Rijke tube are open and modeled with reflection coefficients $R_u = R_d = -1$. The flame is placed between an upstream duct of length $L_u = 0.25$ m and a downstream duct of length L_d that is varied from 0.75 m to 2.0 m in a parameter study. The speed of sound in the upstream duct is $c = 341$ m/s. The flame dynamics are modeled by the FIR shown in Figure 3 and standard acoustic Rankine-Hugoniot jump conditions [25, 26] with a temperature jump $T_d/T_u = 4.96$ and constant isentropic exponent $\gamma = 1.4$. The complete CSS model of the Rijke tube was obtained with the open source software taX[4] [10].

Figure 7 (left) shows the pole map of the Rijke tube obtained with the third-order-upwind-PE CSS model with spline interpolated FIR. The length of the downstream duct varies from 0.75 m (black

[4]https://gitlab.lrz.de/tfd/tax

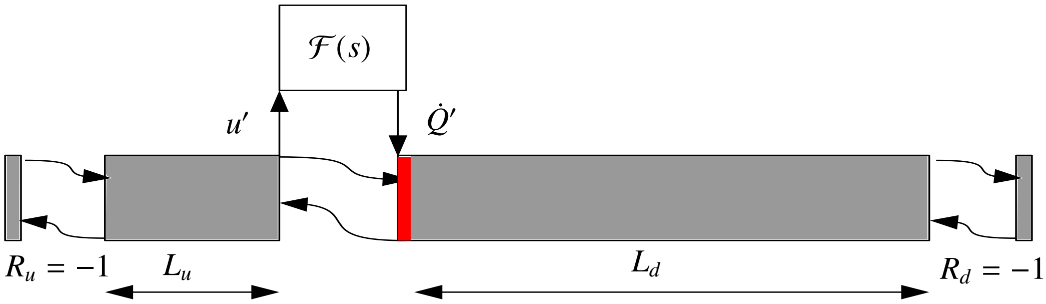

Figure 6: Low-order acoustic network model of a Rijke tube.

markers) to 2 m (gray markers). Also indicated are the poles and zeros of the flame model in red. The blue squares indicate the eigenvalues of the original non-linear problem with $L_d = 0.75$ m, i.e. exponential expressions for the phase shifts due to acoustic wave propagation in the ducts and the time-delayed behavior of the flame, as obtained with an iterative solver assuming the CSS eigenvalue spectra as initial condition. Figure 7 (right) shows the same information for a Rijke tube, where the flame was modeled with the rational fit CSS. In contrast to the rational fit based CSS model of the flame, the PE-based CSS model of the flame has no pole in the investigated region of the complex plane since upwind discretization of the PE guaranties stability and highly damped poles.

For normalized growth rates $\sigma/(2\pi) > -50$ 1/s, the predicted trajectories of the poles of the Rijke tube for both models agree well. According to Figure 5, this is the region of the complex plane where the FTFs of the third-oder-upwind-PE CSS and rational fit CSS agree well with the FTF of the original time-delayed flame model. In contrast, in the region -80 1/s $< \sigma/(2\pi) < -50$ 1/s, 0 Hz $< \omega/(2\pi) <$ 500 Hz, where the FTFs of the third-order-upwind-PE CSS and rational fit CSS differ significantly, the PE-based Rijke tube model predicts three additional poles. These additional poles are located close to zeros of the FTF and two of them depend only weakly on the length of the downstream duct. Since these poles do not converge towards a solution of the non-linear Rijke tube model, they are most likely a consequence of the PE discretization and of spurious nature.

Looking at the modes close to the stability border $\sigma = 0$, it seems possible that a less accurate flame model can lead to wrongly predicted instability. It is emphasized that the CSS model must capture

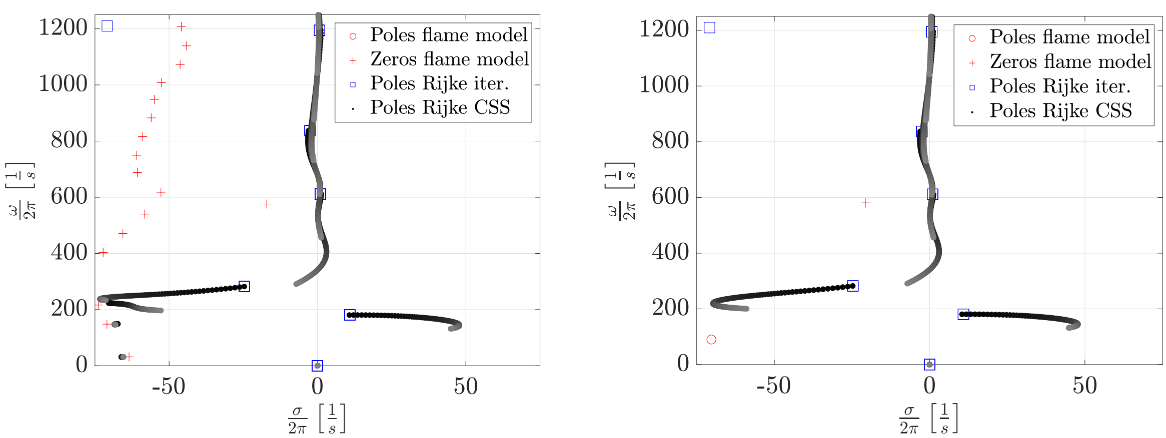

(a) Third-oder-upwind-PE CSS flame model.

(b) Sixth-order rational fit CSS flame model.

Figure 7: Poles of the Rijke tube are shown for a variation of the downstream duct length from $L_d = 0.75$ (black) to $L_d = 2.0$ (gray). Also shown in red are the poles and zeros of the applied flame model. Blue squares indicate poles confirmed by iterative solution of the non-linear model for $L_d = 0.75$.

the phase of the flame response sufficiently well, since thermo-acoustic instabilities are sensitive to the timing between acoustic pressure and heat release fluctuations (Rayleigh criterion) [27]. This underlines that a third-order discretization of the PE is preferable despite its more complicated pole pattern than a first-order PE CSS model.

5. SUMMARY, CONCLUSION AND OUTLOOK

A continuous state-space (CSS) realization of discrete flame impulse responses allows to formulate thermoacoustic stability analysis as a linear eigenvalue problem. The present paper closes the gap between state-space realizations of the simplistic n-τ flame model based on a propagation equation (PE) [11, 13] and more realistic flame models based on rational-fitting [12, 16–18].

The distributed-time-delayed response of flames to velocity perturbations was linearly approximated by discretizing a propagation equation (PE) in pseudo space. We showed that PE-based CSS models lead to rational flame transfer functions, too, and presented an explicit analytical expression for the flame transfer function of the first-order-upwind-PE CSS. Comparison of numerical results demonstrated very good performance of the rational-fitting approach, as it leads to state-spaces models that are two orders of magnitude smaller than PE-based realizations with comparable accuracy. On the downside, the rational fits must be constrained to poles in the negative real half-plane for stability reasons and an increase in the degrees of freedom of the rational function does not guarantee a better fit but can lead to over-fitting of the data. Hence, for parametric studies that require repeated evaluation of CSS models of flame dynamics, the upwind-PE approach is preferable, since it guarantees stability of the state-space model of the flame. Furthermore, the quality of the model is guaranteed to increase with state-space size. It is preferable to discretize the PE with a third-order upwind stencil in order to achieve an accuracy that is comparable to rational-fitting based CSS. For a generic Rijke tube, spurious modes where found close to the zeros of the PE CSS model of the flame. This phenomenon should be kept in mind when analyzing eigenvalue spectra obtained by PE-based CSS models and needs further investigation.

In addition to the PE and rational-fitting strategy, control theory knows many techniques to realize a state-space model from the discrete impulse response (Markov parameters) of a system. The central tool in these strategies is a singular value decomposition of the Hankel matrix [22]. In the present study, these techniques were not further investigated since they lead to a time-discrete state-space model. However, for acoustic networks based on time-discrete state-space models, these methods can prove useful and should be considered. For an application in the context of acoustics see Pelling and Sarradj [28]. A direct comparison with the PE CSS model presented here can be the scope of further work.

ACKNOWLEDGEMENT

This project has received funding from the European Union's Horizon 2020 research and innovation programme under Grant Agreement No 765998 *Annular Instabilities and Transient Phenomena in Gas Turbine Combustors* (ANNULIGhT).

REFERENCES

[1] T. Lieuwen. Modeling Premixed Combustion - Acoustic Wave Interactions: A Review. *Journal of Propulsion Power*, 19(5):765–781, 2003.

[2] Wolfgang Polifke. Black-Box System Identification for Reduced Order Model Construction. *Annals of Nuclear Energy*, 67C:109–128, May 2014.

[3] S. Jaensch, C. Sovardi, and W. Polifke. On the Robust, Flexible and Consistent Implementation of Time Domain Impedance Boundary Conditions for Compressible Flow Simulations. *Journal of Computational Physics*, 314:145–159, June 2016.

[4] Wolfgang Polifke. Modeling and Analysis of Premixed Flame Dynamics by Means of Distributed Time Delays. *Prog. Energy Combust. Sci.*, 79:100845, 2020.

[5] Xiaodong Jing and Xiaofeng Sun. Experimental investigations of perforated liners with bias flow. *The Journal of the Acoustical Society of America*, 106(5):2436–2441, November 1999.

[6] F. Nicoud, L. Benoit, C. Sensiau, and T. Poinsot. Acoustic Modes in Combustors with Complex Impedances and Multidimensional Active Flames. *AIAA Journal*, 45(2):426–441, 2007.

[7] Philip E. Buschmann, Georg A. Mensah, Franck Nicoud, and Jonas P. Moeck. Solution of Thermoacoustic Eigenvalue Problems With a Noniterative Method. *Journal of Engineering for Gas Turbines and Power*, 142(3), March 2020.

[8] Moritz Merk, Philip E. Buschmann, Jonas P. Moeck, and Wolfgang Polifke. The nonlinear thermoacoustic eigenvalue problem and its rational approximations: assessment of solution strategies. In *Proceedings of the ASME Turbo Expo 2022*, Rotterdam, The Netherlands, 2022. ASME (accepted for publication).

[9] B. Schuermans, V. Bellucci, and C. O. Paschereit. Thermoacoustic Modeling and Control of Multi-Burner Combustion Systems. In *Proceedings of the ASME Turbo Expo 2003, collocated with the 2003 International Joint Power Generation Conference*, GT2003-38688, pages 509–519, Atlanta, GA, USA, 2003. ASME.

[10] Thomas Emmert, Max Meindl, Stefan Jaensch, and Wolfgang Polifke. Linear State Space Interconnect Modeling of Acoustic Systems. *Acta Acustica united with Acustica*, 102(5):824–833, 2016.

[11] Max Meindl, Thomas Emmert, and Wolfgang Polifke. Efficient calculation of thermoacoustic modes utilizing state-space models. In *23nd Int. Congress on Sound and Vibration (ICSV23)*, Athens, Greece, 2016.

[12] P. Subramanian, R. S. Blumenthal, R. Sujith, and W. Polifke. Distributed Time Lag Response Functions for the Modelling of Combustion Dynamics. *Combustion Theory and Modelling*, 19(2):223–237, February 2015.

[13] Herbert Mangesius and Wolfgang Polifke. A discrete-time, state-space approach for the investigation of non-normal effects in thermoacoustic systems. *Int. J. Spray Comb. Dynamics*, 3(4):331–350, 2011.

[14] Martin Schmid, Ralf Blumenthal, Moritz Schulze, Wolfgang Polifke, and Thomas Sattelmayer. Quantitative Stability Analysis Using Real Frequency Response Data. *Journal of Engineering for Gas Turbines and Power*, 135(12):121601, 2013.

[15] Q. Douasbin, C. Scalo, L. Selle, and T. Poinsot. Delayed-time domain impedance boundary conditions (D-TDIBC). *Journal of Computational Physics*, 371:50–66, 2018.

[16] Felix Schily, Thomas Komarek, and Wolfgang Polifke. A criterion for thermo-acoustic stability based on the flux of acoustic energy. *Combustion and Flame*, 227:238–254, May 2021.

[17] A. Avdonin, Max Meindl, and W. Polifke. Thermoacoustic analysis of a laminar premixed flame using a linearized reacting flow solver. *Proceedings of the Combustion Institute*, 37:5307–5314, 2019.

[18] Max Meindl, Alp Albayrak, and Wolfgang Polifke. A state-space formulation of a discontinuous Galerkin method for thermoacoustic stability analysis. *Journal of Sound and Vibration*, 481:115431, 2020.

[19] Mirko Bothien, Jonas Moeck, Arnaud Lacarelle, and Christian Oliver Paschereit. Time Domain Modelling and Stability Analysis of Complex Thermoacoustic Systems. *Proceedings of the*

Institution of Mechanical Engineers, Part A: Journal of Power and Energy, 221(5):657–668, January 2007.

[20] James R. Leigh. *Control theory: a guided tour*. Number 72 in IET control engineering series. The Inst. of Engineering and Technology, London, 3. ed edition, 2012.

[21] V. N. Kornilov, R. Rook, J. H. M. ten Thije Boonkkamp, and L. P. H. de Goey. Experimental and Numerical Investigation of the Acoustic Response of Multi-Slit Bunsen Burners. *Combustion and Flame*, 156(10):1957 – 1970, October 2009.

[22] Athanasios C. Antoulas. *Approximation of Large-Scale Dynamical Systems*. Society for Industrial and Applied Mathematics, January 2005.

[23] H. Padé. Sur la représentation approchée d'une fonction par des fractions rationnelles. *Annales scientifiques de l'École normale supérieure*, 9:3–93, 1892.

[24] MATLAB, Version R2021b, Copyright 2009-2020 The MathWorks, Inc.

[25] Thomas Emmert, Sebastian Bomberg, and Wolfgang Polifke. Intrinsic Thermoacoustic Instability of Premixed Flames. *Combustion and Flame*, 162(1):75–85, 2015.

[26] Boa-Teh Chu. On the generation of pressure waves at a plane flame front. *Symposium (International) on Combustion*, 4(1):603–612, January 1953.

[27] John William Strutt Rayleigh. *The theory of sound. Vol. 2*. Dover classics of science and mathematics. Dover Publ, New York, repr. of 2. ed. rev. and enl., 1894 edition, 1969. OCLC: 830808857.

[28] Art J. R. Pelling and Ennes Sarradj. Efficient Forced Response Computations of Acoustical Systems with a State-Space Approach. *Acoustics*, 3(3):581–594, August 2021.